Pergamon

Int. J. Heat Mass Transfer. Vol. 40, No. 3, pp. 519–532, 1997

0017-9310/97 $15.00+0.00

PII: S0017-9310(96)00166-4

Nucleate pool boiling from coated surfaces in saturated R-134a and R-407c

SHOU-SHING HSIEH and CHUN-JEN WENG

Department of Mechanical Engineering, National Sun Yat-Sen University, Kaohsiung, Taiwan 80424, Republic of China

(*Received* 21 *December* 1995 *and in final form* 23 *April* 1996)

Abstract—Pool nucleate boiling heat transfer experiments from coated surfaces immersed in saturated R-134a and R-407c with porous aluminum, copper, molybdenum, and pitted coating on a copper surface were conducted. The influence of coating thickness and porosity on heat transfer and boiling hysteresis were studied. The enhanced surface heat transfer coefficients are 2.5 times higher than those of the smooth surface. Furthermore, the effects of refrigerant thermophysical properties are also presented and discussed. The experimental data for plasma and flame spray coating surfaces were correlated in terms of the Reynolds number based on a mean pore diameter and porosity, Jakob number, constant heat flux number and geometric scale factor to provide a thermal design basis for engineering application. Copyright © 1996 Elsevier Science Ltd.

INTRODUCTION

Many water chillers of the centrifugal type have evaporators utilizing a flood type of operation whereby the water is circulated through the tube and refrigerant evaporated on the shellside of the tubes which is an area of nucleate boiling. While designing the evaporator of such a system, one must be able to accurately predict the boiling heat transfer coefficients of the refrigerants used. However, the prediction of the heat transfer coefficient is difficult because the boiling phenomenon is rather complex and is influenced by many variables, such as surface conditions, heater size, geometry, material, and refrigerants, etc. In addition, most refrigeration systems are expected to perform at a high coefficient of performance and energy efficiency. One method of achieving this goal is to enhance the boiling heat transfer coefficient between the refrigerant and the heat source in the evaporator.

Various methods of enhancing nucleate boiling heat transfer have been described by Thome [1] and Webb [2]; both provided a comprehensive survey, and discussed the fundamental phenomena of boiling on enhanced surfaces. These surfaces can take a number of forms from simple low integral fins with varying fin profile to more complicated re-entrant cavity type surfaces such as structured and porous coated surfaces. Although a considerable amount of published data exists in the literature on nucleate boiling enhancement, little study has been done on the effects of coating/painting techniques on these surfaces. Recently, O'Connor and You [3] developed a boiling heat transfer enhancement paint by increasing the number of active nucleation sites.

The effects of porous media on the mechanism of boiling heat transfer phenomena have been studied for a number of different media and surface conditions. Typically, the porous medium is composed of small spheres of various materials or of fibrous wicking materials. The results of the various studies indicate that the nature of the characteristic boiling curve depends on some measure of the pore size in the media. One of the first surfaces developed specifically to enhance nucleate pool boiling was the porous sintered metallic coating of Thome [1]. The 'particle spraying' technique was recently applied by You *et al.* [4] to a flat horizontal surface with a 0.3–3 μm Al_2O_3 particle. In spite of this, a complete understanding of the surface microstructure effect on nucleate boiling heat transfer is still essentially needed, and the mechanisms through which boiling heat transfer enhancements are made should be to obtain further knowledge regarding boiling in the presence of liquid-saturated porous layer.

In recent years, environmental concerns over the use of CFCs as working fluids in refrigeration and air-conditioning plants have led to the development of alternative fluids. Among these alternatives, R-134a is seen as a replacement for the commonly used CFC-12 and R-407c is to be a substitute for HCFC-22. Moreover, considerably recent effort has been made in finding ways to design more compact and efficient evaporators for the process and refrigeration industries based on CFCs/non-CFCs. Industries are currently undergoing a massive conversion process from CFC to HCFC/or HFC. The conversion establishes a need for refrigerant data on the replacement refrigerants such as R-134a and R-407c used in this study. The objective of the paper is to develop a surface

NOMENCLATURE

A	heat transfer area [m^2]
$\bar{A}$	9.7 $P_c^{0.5}$ [bar] in Fig. 5
b	$[2\sigma/g(\rho_l-\rho_v)]^{0.5}$ Laplace constant
C_p	specific heat [kJ kg^{-1} K^{-1}] at constant pressure
D	outside diameter of test tube [mm]
d_e	equilibrium break-off-diameter ($d_e=0.146\beta$b) in Fig. 5 [m]
$F(p)$	$1.8P_r^{0.17}+4P_r^{1.2}+10P_r^{10}$ pressure function in Fig. 5
g	acceleration of gravity [m s^{-2}]
h	heat transfer coefficient [W m^2 K^{-1}]
h_{lv}	latent heat [kJ kg^{-1}]
Ja	Jakob number, $Ja=C_{pl}\Delta T/h_{lv}$
k	thermal conductivity [W m^{-1} K^{-1}]
L	length of test tube [mm]
P	pressure [kPa]
P_c	critical pressure [bar]
P_r	reduced pressure, P/P_c
N_{cf}	constant heat flux number, $N_{cf}=\mu_l^2/\eta\rho_l\sigma$
Q	heat transfer rate [W]
Ra	roughness [μm]
Re	Reynolds number, $Re=q\eta/h_{lv}\mu_l\varepsilon$
q	heat flux (Q/A) [W m^{-2}]
r_b	embryonic bubble radius [μm]
T	temperature [K]
ΔT	temperature difference [K].

Greek symbols

α	thermal diffusivity [m^2 s^{-1}]
β	contact angle ($=35°$)
δ	porous layer thickness [μm]
ε	porosity [%]
η	average pore diameter [μm]
λ	geometric scale factor, $\lambda=\eta/\delta$
μ	viscosity [kg m^{-1} s^{-1}]
ν	kinematic viscosity [m^2 s^{-1}]
ρ	density [kg m^{-3}]
σ	surface tension [N m^{-1}].

Subscripts

f	refrigerant
l	liquid
s	smooth tube
sat	saturation
v	vapor
w	wall of tube.

treatment that will provide high heat transfer rates in nucleate pool boiling and to enlarge the pool boiling data for alternative refrigerants of R-134a and R-407c.

EXPERIMENTAL APPARATUS AND PROCEDURE

Test facility and test section

The experimental apparatus for the study is shown in Fig. 1. It consists of a cylindrical stainless steel pressure vessel with a volume of $\pi/4\cdot(21.6)^2\times(40)$ cm^3, a stainless steel side panel provided with ports for electric wires, a pressure gauge and thermocouples, a vacuum pump, a reflux condenser, auxiliary heaters (or thermostat baths), and a test-section support. Insulation was peripherally provided on the outside of the tank. The evaporator tube was designed to simulate a portion of a typical rod in refrigerant-flooded evaporator, it was fabricated from a copper tube. The tube specimen is soldered to a flange at one end of the tank. The copper tubes were 19 mm in outer diameter, with an inner diameter of 11 mm. Each cartridge heater was 350 mm long (actual heated length is 330 mm) and 10.95 mm in diameter with a maximum power output of 2 kW and was inserted into the copper tube. A detailed description of the cartridge heater can be found from Hsieh and Hsu [5]. The test section included both smooth and treated surfaces. The dimensional specifics of the surfaces treated are given in Table 1.

The ten test specimens studied had the general characteristics shown in Fig. 1. Four holes of 1.2 mm diameter and 70 ~ 100 mm deep were drilled at each end of the cylinders at 90° intervals with the axis within about 1.2 mm of the smooth surface for insertion of wall temperature thermocouples. The cylinders with coating surfaces were provided by the Metal Industrial Research and Development Center (MIRDC) of Taiwan and are designated as test sections 1s, 2p, 3p, 4_F, 5_F, 6_F, 7c, 8c, 9c, and 10c. Test section 1s has a plain/smooth surface while the other test sections were coated with: plasma spray (2p and 3p), flame spray (4_F, 5_F, and 6_F), and pitted coating (7c, 8c, 9c, and 10c). The porosity (ε), thickness of porous layer (δ) and mean pore diameter (η) of the coated surfaces were calculated according to photographs of the polished samples using an image analysis software like OPTIMAS provided by Industrial Technology Research Institute (ITRI) of Taiwan, and the surface roughness (Ra) was measured by a profile measuring device and readout by a Surfcorder SE-3000 developed by Losaka Laboratory Ltd. The detailed characteristics of the coated surfaces and the dimensions of the tubes tested are also listed in Table 1.

Calibrated copper–constantan sheath thermo-

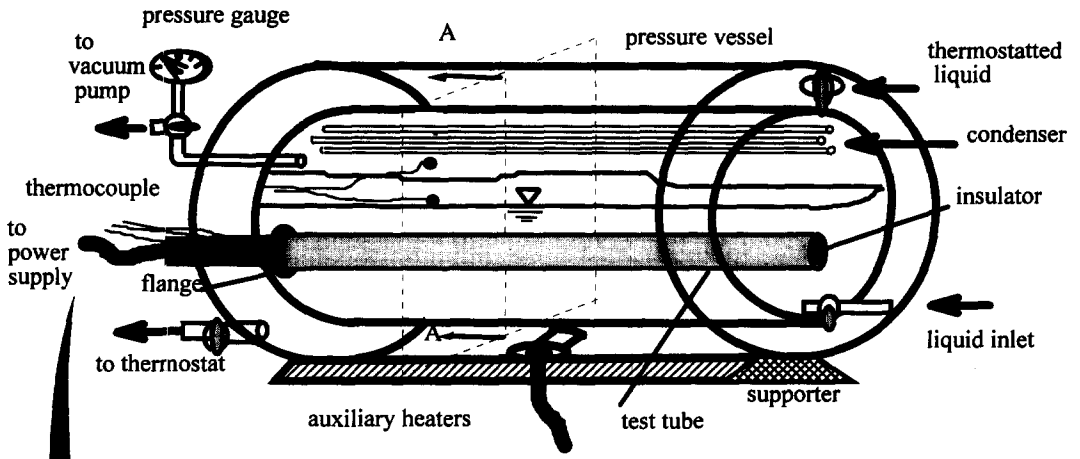

(a) Test section

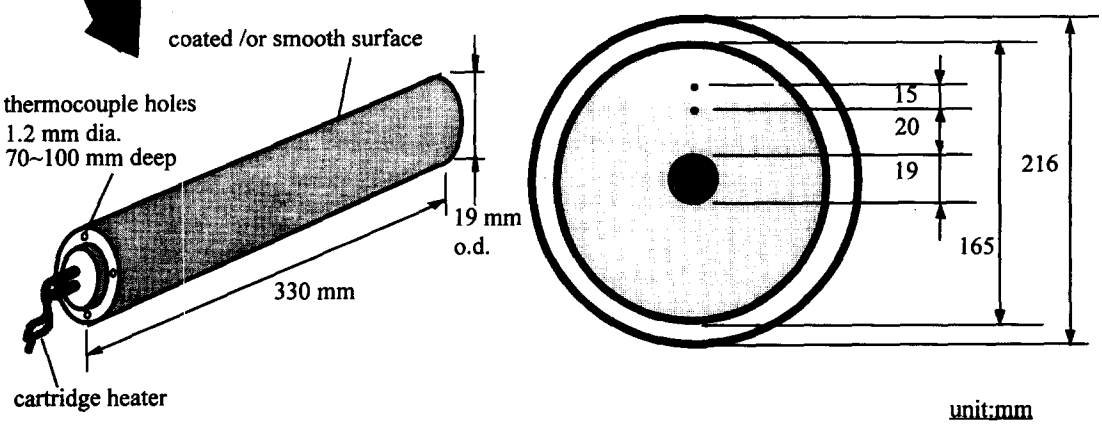

Section A-A

(b) Thermocouple locations and test specimen

Fig. 1. Pool boiling apparatus setup.

couples of diameter 1.1 mm were employed to measure the wall temperature. To minimize longitudinal heat conduction, silicon rubber and Devon five-minute epoxy glue mixed with polystyrene foam were applied at the ends for the use with R-134a and R-407c. The liquid temperature in the evaporator was measured by two thermocouples placed close to the free surface of the liquid. The temperature difference between these two points was between ± 0.1°C at the maximum power input. Another thermocouple, used to measure the vapor temperature, was positioned midway along the evaporator about 15 mm above the liquid surface.

Test procedure

Prepared test sections were cleaned with chlorinol and water and finally, with acetone. The tank was cleaned with acetone before each run. Once the evaporator tube was installed, the system was evacuated to a pressure of about 30 Pa. If no leaks were detected over a 24 h interval, then the evaporator was charged with the working fluid from the reservoir to a level 20 mm above the top of the tube. Power was given to the pool to de-gas the test fluid R-134a and R-407c at a heat flux of 50 kW m^{-2} for 1.5 h, this results in a vapor pressure of 343.06 kPa (R-134a) and 658.61 kPa (R-407c). The saturation temperature at the measured

Table 1. The specifications and dimensions of treated surfaces

Designated symbol	Types of coating	Surface (coating material)	Diameter of test tube D [mm]	Thickness of porous layer δ [μm]	Surface roughness Ra [μm]	Porosity ε	Mean pore diameter η [μm]
1s	—	Smooth	19	—	0.03	—	—
2p	Plasma	Cu	19	35	6.79	0.077	5
3p	Spraying	Mo	19	100	11.30	0.080	2
4_F		Al(L)	19	50	10.28	0.037	3
5_F	Flame Spraying	Al(H)	19	300	13.58	0.026	5
6_F		Zn	19	150	8.90	0.113	1
7c		#20	19	30	4.57	—	—
8c	Pitted	#50	19	18	3.95	—	—
9c	Coating*	#100	19	31	2.12	—	—
10c		#150	19	32	1.82	—	—

Symbol: s, smooth; p, plasma coating; F, flame spray; c, pitted coating; *, emery particle; #, mesh number; L, low roughness; H, high roughness.

Table 2. Properties of R-134a and R-407c at $T_{sat}=4.4°C$ (data from ICI)

Properties	R-134a	R-407c
Composition (formula)	$CH_2F\text{-}CF_3$	R-32/125/134a (23/25/52) wt%
Substitute for	R-12	R-22
ODP [R-11 = 1.0]	0	0
GWP [R-11 = 1.0]	0.26	0.39
Flammability	no	no
Toxicity [AEL(TLV)] [ppm]	1000	1000
Boiling temperature at 1 atm [°C]	−26	−36.8 to −44.0 Glide approx 5°C
Critical temperature [°C]	101	87
Lubricant (compressor)	(Polyol-) Easter	(Polyol-) Easter
ρ_l [kg m^{-3}]	1280.230	1218.900
ρ_v [kg m^{-3}]	16.781	22.251
C_{p_l} [kJ kg^{-1} K^{-1}]	1.358	1.408
C_{p_v} [kJ kg^{-1} K^{-1}]	0.795	0.790
h_{lv} [kJ kg^{-1}]	193.707	209.056
k_l [W m^{-1} K^{-1}]	0.093	0.099
μ_l [cP]	0.259	0.211
σ [N m^{-1}]	0.011	0.009
Molecular weight	102.030	86.170
Boiling point [bar]	3.421	—
Dew point pressure [bar]	—	5.356
Bubble point pressure [bar]	—	6.566

Note: ODP, ozone depletion potential; GWP, global warming potential; AEL, allowable exposure limit; TLV, threshold limit value.

pressure was compared to the pool temperature measured by the thermocouple. Both increasing and decreasing heat flux data were taken in order to observe boiling hysteresis. For the decreasing data, the heat flux was reduced from 70 kW m^{-2} in predetermined steps by means of a variac.

During all the tests, the saturation temperature was kept near 4.4°C for R-134a and R-407c supplied by ICI (Imperial Chemical Industries) Chemicals & Polymers Limited. More detailed relevant properties of the refrigerants in this study are given in Table 2. All the data were obtained and reduced with a computer-controlled data acquisition system.

Enhancement coating and its preparation

The boiling enhancement coating used for the present surface treatment includes three types of coatings. They are so called plasma spraying, flame spraying and pitted coatings. A scanning electron microscope (SEM) image of several typical treated surfaces is depicted in Fig. 2.

The substrate material used in the present study was copper. The surfaces of the test copper tubes were first polished by an emery paper. Plasma spraying of Cu and Mo was carried out using PT-F4 plasma gun at 28–52.5 kW power. The plasma jet is about 5–10 cm long and the nozzle–substrate distance is about 14

(a) Cu (×5000)-top ⊢ 1μm

(b) Mo (×5000)-top ⊢ 1μm

(c) Al(L) (×5000)-top ⊢ 1μm

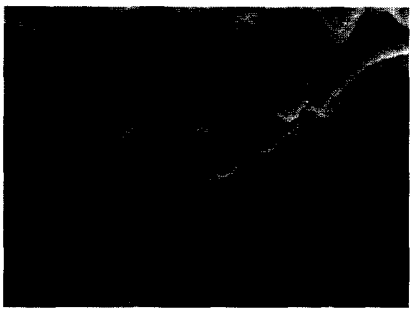

(d) Zn (×5000)-top ⊢ 1μm

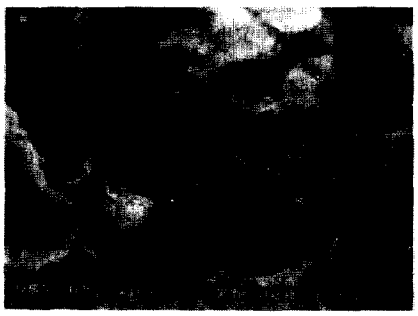

(e) #150 (×5000)-top ⊢ 1μm

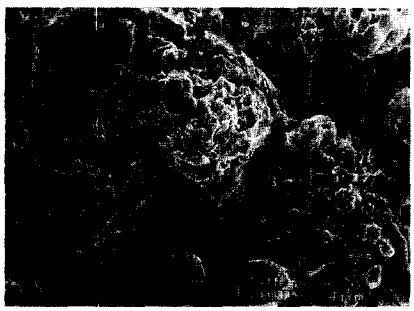

(f) Mo (×1000)-top ⊢ 10μm

(g) Mo (×1000)-side ⊢ 10μm

Fig. 2. SEM photographs of enhanced tube microstructure.

cm. The carrier gas is Ar + H_2 flowing typically at 4 l min^{-1}. Helium was added to increase gas flow and Cu and Mo powders with grain sizes 45–135 μm were used. The plasma condition was: a 750 A arc current, a 310 g h^{-1} powder feed rate, a substrate temperature of 200°C and a 14 cm spraying distance. A traditional oxy-fuel gas C_2H_2 flame with a METCO 12E gun was used for flame spraying of Al and Zn spray distance about 15 cm. Coating thickness ranges from 50–300 μm. Four different numbers of meshes of the pitted particles were treated with pitted coating using a sand blasting technique, which results in a larger particle size (smaller mesh number) having a higher surface roughness. Table 1 gives more detailed data regarding the three types of surface treatments in the present study.

Precautions taken during experiments

In measuring boiling heat transfer coefficients, great care must be exercised to ensure good accuracy. The following listings are those precautions:

(1) The pool temperature was compared to the saturation temperature corresponding to the measured saturation pressure for pure refrigerants. This ensures that there are no non-condensibles in the system. It also verifies that there is no subcooling in the liquid pool within ±0.2°C.

(2) The heater was tested for circumferential uniformity of heat flux. To smooth out any non-uniformities in the heat flux caused by the cartridge heater, a copper sleeve with a two-walled sink compound was used inside the test-tube into which the cartridge heater was inserted with a tight mechanical fit. The outer diameter of the sleeve was machined to the inside diameter of the test tube. Its center was bored out to accommodate the cartridge heater.

(3) To ensure that the correct wall temperature was measured, a thermocouple was tightly-pressed onto the wall in a sleeve insert with thermal jointing compound applied to the tube. The variation of the thermocouple reading was found to be less than 0.1°C at $q_{max} = 62$ kW m^{-2}.

The average wall temperature was used to define the heat transfer coefficient. It is defined using the average value of the four wall thermocouples. The heat flux is based on the heated area of the tube which was in contact with the liquid.

Uncertainty estimates

An error analysis as suggested by Moffat [6] was made considering the errors of the instruments, the measurement variance, geometric uncertainty and calibration errors for the heat flux and temperature measurements. The resultant uncertainties for the relevant parameters considered in the study were listed in Table 3.

Table 3. Uncertainty estimates

Parameter	Uncertainty
Minimum heat flux $q_{min} = 0.60$ kW m^{-2}	±8.7%
Maximum heat flux $q_{max} = 62$ kW m^{-2}	±1.2%
Heat transfer area A	±0.3%
Wall temperature T_W at q_{min}	±1.0%
Wall temperature T_W at q_{max}	±0.3%
Saturation temperature $T_{sat} = 4.4$°C	±1.0%
Superheat temperature ΔT at q_{min}	±5.7%
Superheat temperature ΔT at q_{max}	±1.6%
Heat transfer coefficient h at q_{min}	±10.4%
Heat transfer coefficient h at q_{max}	±2.0%

RESULTS AND DISCUSSION

A typical result of JSM-6400 SEM examination for the surface images of 2p, 3p, 4_F, 5_F and 10c is illustrated in Fig. 2(a)–(e), respectively. The distribution appears rather random in these micrographs (× 5000). In addition, Fig. 2(f)–(g) exhibits SEM images (× 1000) of the 3p coating upper surface and side view, respectively. The microstructures are layered with a total thickness ≈ 100 μm and results in a cavity size of about 2 μm. Again, surface orientation is random, some lying vertically and some horizontally, which produces a porous microstructure with a mean pore diameter of 2 μm and a porosity of 0.08. Generally speaking, it seems to have a large variation in pore size and shape, as shown in Fig. 2, in which it probably functions as a vapor escape passage.

The present heat transfer characteristics were governed by porous layer thickness, the pore diameter, the surface porosity, the contact angle and their combined complex effect. Figure 3 compares pool boiling data for the smooth (1s) and coated surfaces at identical bulk liquid conditions for R-134a. The contact angles of most industrial materials with R-134a are nearly the same. The surface porosity of these two types of coatings (plasma and flame spraying coating) are only slightly different. It seems, therefore, that the parameters with the most influence are the porous layer thickness and the pore diameter of the treated surface, which determines the probability of flooding the re-entrant cavities and the degree of superheat required for bubble growth. The observed differences in the boiling curves are indications of variations in the surface microstructures between the smooth and coated surfaces. The data show that the hysteresis phenomenon can be observed for both smooth and enhanced surfaces. However, the hysteresis effect of the coated surfaces seems stronger than that of the smooth surface.

The phenomenon of the onset of nucleate boiling for smooth and porous surfaces is completely different for each surface, as pointed out by Afgan *et al.* [7]. Upon incipience, for a smooth surface, the separation of a bubble from the superheated boundary layer adjacent to the tube wall into the relatively colder fluid is considerably impeded. This results in a decrease in active nucleation sites. In fact, when the top of the bubble leaves the superheated boundary layer adjacent to the tube wall and touches the cold liquid, the bubble growth ceases, or slows down. While, for

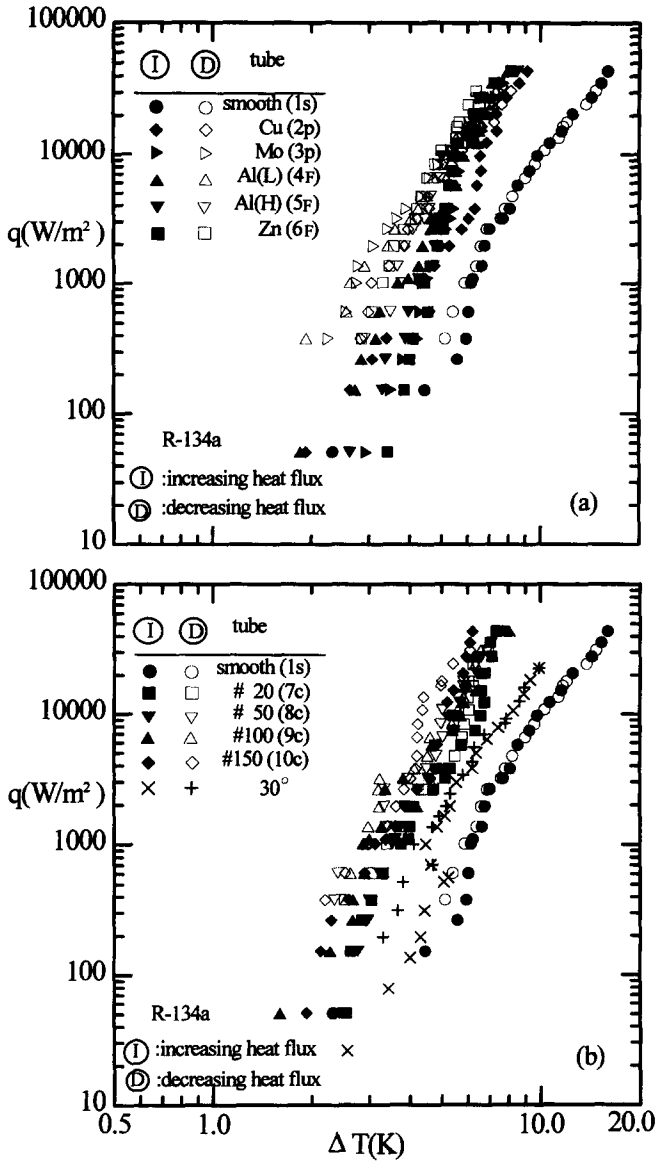

Fig. 3. Boiling curves of the enhanced tubes for R-134a.

porous surfaces, there seems to be a tunnel like system in the open pore structure. At this stage, the cross section of a nucleation site looks like a cylindrical tunnel and liquid evaporation takes place on the surface of the meniscus on its boundaries. Intensive evaporation occurs due to the extended evaporation surface and the great liquid superheating inside the porous structure. Meanwhile, the active nucleation site in fact functions as a small 'heat pipe'. The intensive feeding of the growing bubble with vapor through the tunnel of the heat pipe will take place until its separation from the wall. This is why the bubble generated on a surface with a porous layer, such as the coated surfaces (2p, 3p, 4_F, 5_F and 6_F), in a relatively cold liquid, grows without difficulty, as shown in Fig. 3(a). Based on the reasons stated above, intensive bubble boiling on porous surfaces will commence for R-134a and R-407c at a lower degree of superheat than for smooth surfaces, see Table 4. The boiling behavior of enhanced surfaces, like 7c, 8c, 9c and 10c (as shown in Fig. 3(b)), seems to have a different surface microstructure than for a porous surface, as shown in Fig. 3(a).

The boiling curve in Fig. 3(a) shows that the performance of the enhanced tubes is nearly the same when the heat flux q is beyond 10 kW m^{-2} for plasma coatings (2p and 3p) and flame spray surfaces (4_F, 5_F and 6_F). Furthermore, the performance difference between plasma and flame sprays seems not to be clearly noted. However, in Fig. 3(b) below this value

Table 4. Degree of superheat for different tubes

Tube	Degree of superheat ΔT [K] R-134a ΔT [K]	R-134a r_b [μm]*	R-407c ΔT [K]	R-407c r_b [μm]*
Smooth (1s)	6.5	0.255	8.0	0.096
Cu (2p)	5.8	0.276	2.7	0.330
Mo (3p)	4.7	0.352	3.0	0.294
Al(L) (4_F)	4.8	0.343	—	—
Al(H) (5_F)	4.5	0.369	5.0	0.167
Zn (6_F)	5.0	0.328	5.8	0.141
no. 20 (7c)	5.0	0.328	7.0	0.113
no. 50 (8c)	4.8	0.343	—	—
no. 100 (9c)	4.3	0.388	—	—
no. 150 (10c)	4.0	0.421	6.3	0.128

'—' means not available; '*' upon boiling incipience.

(10 kW m^{-2}) the pitted surfaces have a better performance of enhanced heat transfer than those of plasma/flame spray surfaces. This behavior may be explained as follows: the pore diameter of pitted surfaces is larger than for other enhanced surfaces, so the vapor flow resistance through the pore of pitted surfaces is greater. At low heat flux ($q < 10$ kW m^{-2}) the superheat is relatively low, so the vapor pressure is not sufficient to warrant the bubble escaping.

The smooth surface exhibited a slight temperature overshoot and weak boiling hysteresis while a larger temperature overshoot and a stronger hysteresis phenomenon were found with enhanced surfaces especially in R-407c, as shown by typical data in Fig. 4. The liquid penetration into the porous matrix in the R-407c tests should be more than in the R-134a tests for a given enhanced surface. Strong hysteresis phenomena were also observed in R-113 with plasma spray coating by Tehver *et al.* [8]. Table 4 summarizes the degree of superheat for enhanced tubes for R-134a and R-407c; also included is smooth tube data for comparison and reference.

Figure 5 shows the test results for R-134a and R-407c boiling on the ten test surfaces (Fig. 5(a)) and selected surfaces (Fig. 5(b)) in decreasing heat flux mode. The solid lines are the data of Bier *et al.* [9] for a smooth surface. The present result agrees very closely with that of Bier *et al.* for the trend; namely, the same log–log slope of ~ 0.7 but the magnitude of the present work seems much higher due to the enhanced tubes used. At $q > 10$ kW m^{-2}, the R-134a has better heat transfer performance than that of the corresponding coated surface in R-407c. The reason for this behavior is perhaps that an improvement in the heat transfer coefficient at the nucleation site under certain coated surfaces occurs as the surface becomes more wettable in R-134a compared to that of R-407c at a higher heat flux (say, $q > 10$ kW m^{-2}). In addition, in both Fig. 5(a) and (b), results from Stephan and Abdelsalam for smooth surfaces [10] as well as Cornwell and Houston [11] for enhanced tubes were added for comparison.

The enhancement ratio (h/h_s) vs q for R-134a and R-407c was plotted in Fig. 6(a) and (b), respectively. The trend and magnitude seem completely different among the participating surfaces in R-134a and R-407c. The distribution is quite random which of course is due to the rather random nature of the distribution of the active nucleation site for enhanced surfaces. In addition, variations of h/h_s seem milder for plasma/flame sprayed coating surfaces than those for pitted

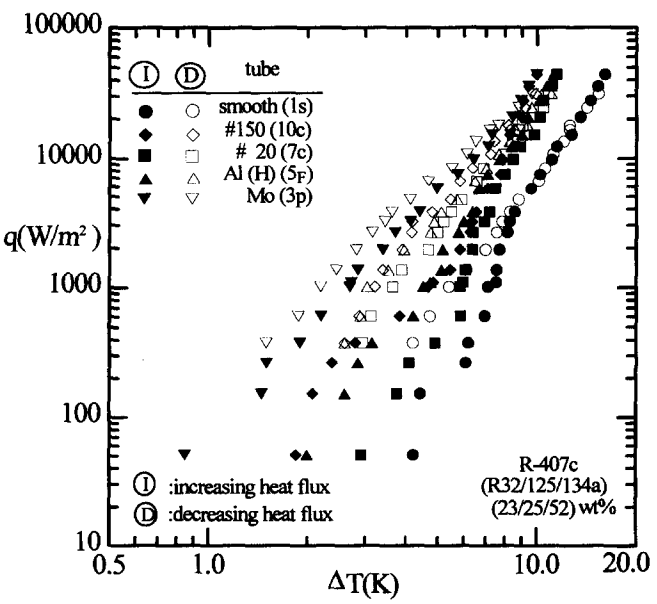

Fig. 4. Boiling curves of enhanced tubes for R-407c.

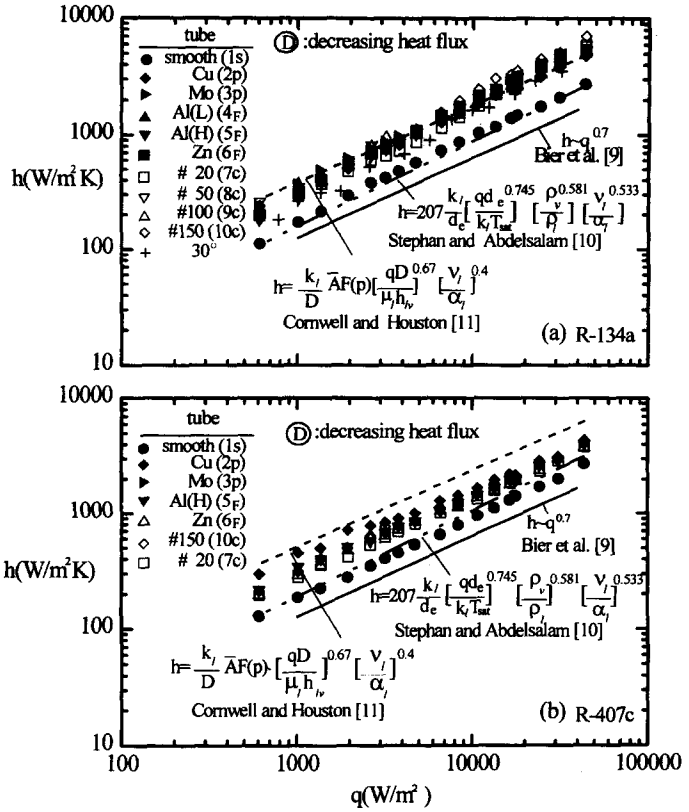

Fig. 5. Heat transfer comparison for R-134a and R-407c.

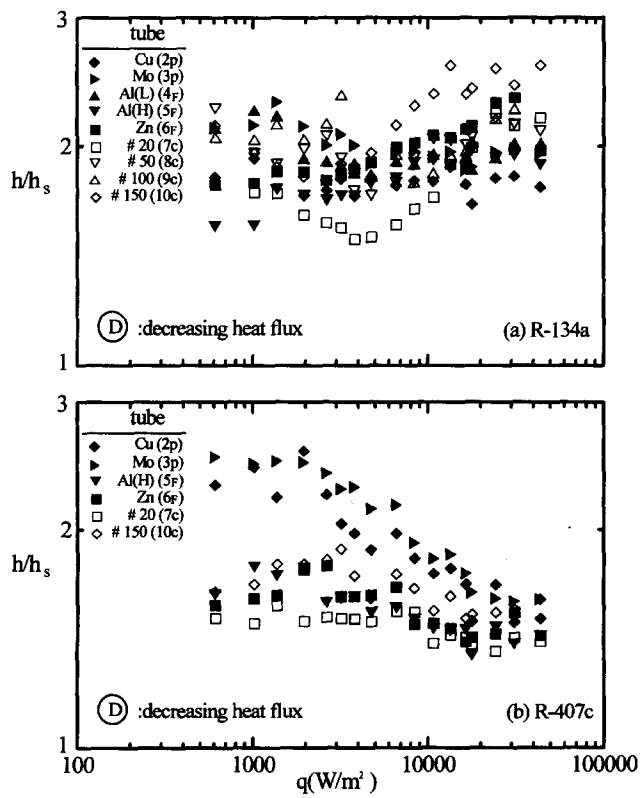

Fig. 6. Effects of enhanced tubes for R-134a and R-407c.

Table 5. Enhancement ratio for various enhanced coating tubes with R-134a and R-407c

Relevant studies	Refrigerant	Coating material	Surface roughness Ra (μm)	h/h_S Heat flux 1.3 kW m^{-2}	10 kW m^{-2}	25 kW m^{-2}
Present study	R-134a	Smooth (1s)	0.03	1.00	1.00	1.00
		Cu (2p)	6.79	1.85	1.79	1.81
		Mo (3p)	11.30	2.30	1.94	1.96
		Al(L) (4_F)	13.58	2.20	1.95	1.93
		Al(H) (5_F)	10.28	1.75	1.92	1.93
		Zn (6_F)	8.90	1.85	2.07	2.29
		no. 20 (7c)	4.57	1.72	1.70	2.22
		no. 50 (8c)	3.95	1.89	2.05	2.18
		no. 100 (9c)	2.12	2.14	1.84	2.19
		no. 150 (10c)	1.82	1.88	2.36	2.56
	R-407c	Smooth	0.03	1.00	1.00	1.00
		Cu (2p)	6.79	2.22	1.74	1.68
		Mo (3p)	11.30	2.49	1.83	1.61
		Al(H) (5_F)	10.28	1.73	1.46	1.47
		An (6_F)	8.90	1.63	1.49	1.44
		no. 20 (7c)	4.57	1.57	1.39	1.36
		no. 150 (10c)	1.82	1.79	1.55	1.54
Malyshenko and Styrikovich [12]	Water	Smooth	—	—	1.00	1.00
		Al_2O_3	—	—	1.75	1.60
Shi and Liu [13]	Water	Smooth	—	1.00	1.00	1.00
		Cr	—	—	—	1.21
		Zn	—	—	—	1.26
		Cu	—	—	—	1.33
	Ethanol	Smooth	—	1.00	1.00	1.00
		Cr	—	—	—	1.21
		Zn	—	—	—	1.52
		Cu	—	—	—	1.98
Ko *et al.* [14]	Water	Smooth	—	1.00	1.00	1.00
		Cu	—	—	1.14	1.60
Scurlock [15]	R-12	Smooth	—	1.00	1.00	1.00
		Al/Si	—	—	4.00	3.40

'—' means not available.

coating surfaces. But, nevertheless, the most important feature of these data are the high improvements in heat transfer coefficients with the enhanced surface—some are up to 150% increased at a specified heat flux, as shown in Fig. 6(b). This is because the porous structure contains more absorbed gases than a smooth surface while the liquid in the pores is uniformly superheated facilitating the formation of the vapor phase in the pore structure, and because it contains numerous nucleation sites due to the network of randomly interconnected tunnels (capillaries) throughout the porous coating. Furthermore, it can be clearly seen that the plasma spraying coated surface is more properly used in R-407c than that used in R-134a. Typical data for these results are tabulated in Table 5 and compared with those from Malyshenko and Styrikovich [12], Shi and Liu [13], Ko *et al.* [14] and Scurlock [15] for porous coated tubes.

Figure 7(a)–(b) shows the influence of porous coating due to surface roughness and porous layer thickness at different heat flux levels in R-134a and R-407c. For surface roughness, the data exhibit a rather random distribution and, consequently, a maximum enhancement ratio cannot be found, as shown in Fig. 7(a). However, for porous layer thickness, a maximum enhancement ratio can be found at $q = 1.3$ kW m^{-2} and $\delta = 100$ μm for both R-134a and R-407c, as shown in Fig. 7(b). The porosity (ε) of the coating surfaces significantly influences boiling phenomenon and heat transfer coefficients, as depicted in Fig. 7(c). This is perhaps because it affects the hydrodynamics of the vapor phase as ε increases at low heat flux, at

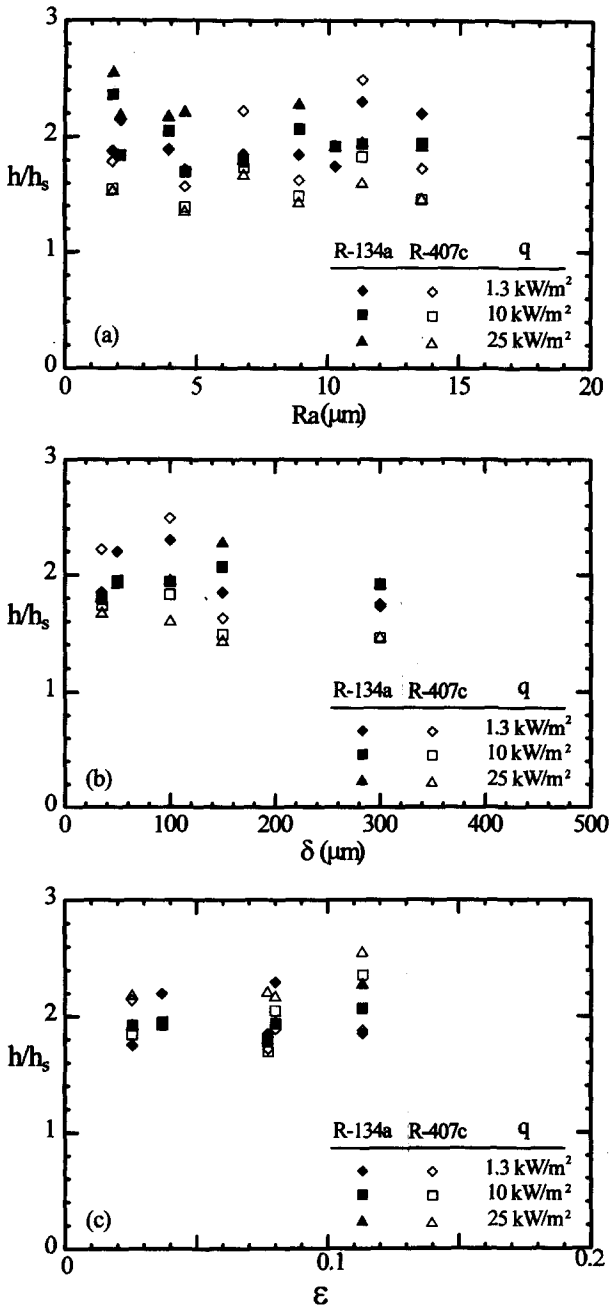

Fig. 7. Influence of porous coating: (a) surface roughness; (b) porous layer thickness; (c) porosity at three different heat flux levels in R-134a/R-407c.

this moment, nucleation is probably inhibited, and the resistance to vapor flow away from the heating surface increases in proportion to the porosity of the porous matrix at low heat flux. While at higher heat flux (say, 25 kW m^{-2}), this situation ceases.

Figure 8 shows typical photographs made by visual observations of the present pool boiling in a smooth surface (1s) and one of plasma spraying surfaces (3p), at two different heat flux levels and two refrigerants (R-134a/R-407c). Starting from Fig. 8(a) in R-134a, one may find that bubble rise from the isolated nucleation site (q = 1.37 kW m^{-2}). As the heat flux increases (q = 5.79 kW m^{-2}) near boiling incipience, more and more sites are activated. At this stage, discrete bubbles less than 1.52 mm in diameter depart from the entire surface, as shown in Fig. 8(b). This small bubble growth and departure behavior was also observed for smooth surface in R-407c as shown in Fig. 8(c)–(d). However, at q = 5.79 kW m^{-2} (see Fig. 8(d)), the departure size of the bubble is about 1.26 mm which is a little bit smaller than those in R-134a at the same heat flux. On the other hand, in Fig. 8(e)–

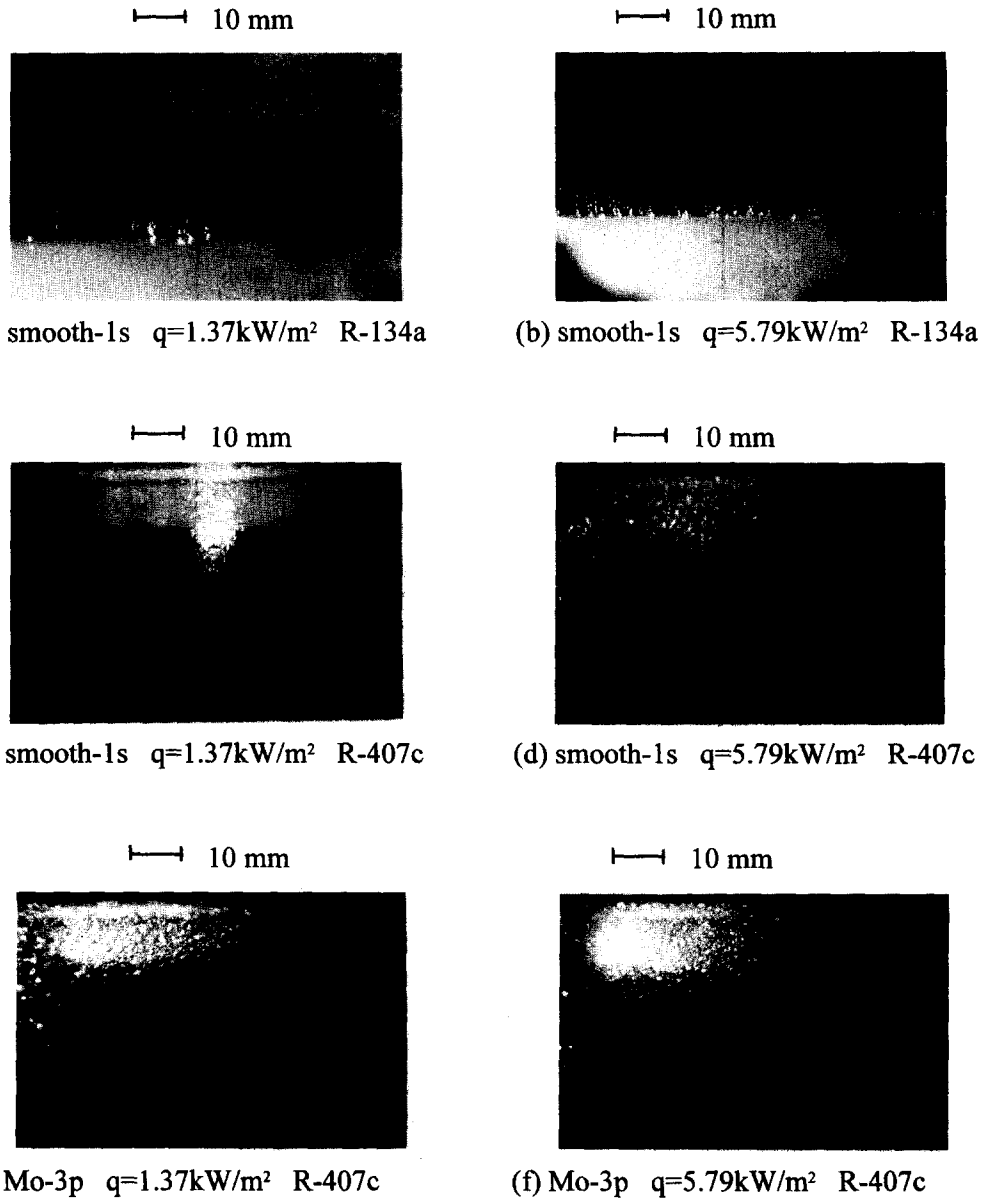

Fig. 8. Visualization of enhanced tube bubble behavior.

(f) for an enhanced surface, the active sites become very numerous and the bubbles start to merge into one another. The photographs also identify an increased nucleation site density even for a lower heat flux ($q = 1.37$ kW m^{-2}), displayed in Fig. 8(e), compared to the smooth surface (1s), as shown in Fig. 8(c), evident by the larger number of isolated bubbles over the surface. At this heat flux ($q = 1.37$ kW m^{-2}) bubble departure size increases but seems still isolated (Fig. 8(e)), and the amount of bubble coalescence around the surface increases with increasing heat flux to $q = 5.79$ kW m^{-2} (Fig. 8(f)). To provide a theoretical background, the embryonic bubble radius can be calculated based on the following relation

$$P_{sat}(T_w) - P_{sat}(T_{sat}) = 2\sigma(T_w)/r_b \quad (1)$$

incorporated with the measured incipient superheats and the calculated results upon boiling incipience also listed in Table 4. It is found that the calculated bubble size for a smooth surface under a certain heat flux level, e.g. Fig. 8(b) and (d), ranged between 0.071 μm and 0.134 μm, and for enhanced surface between 0.122 μm and 0.215 μm as shown in Fig. 8(e) and (f). This increase suggests the ability of the porous coating surface enhancement to trap vapor effectively. This is in good agreement with the apparent structure sizes existing among the range of 0.1–3 μm (see Fig. 2(b) and (d)).

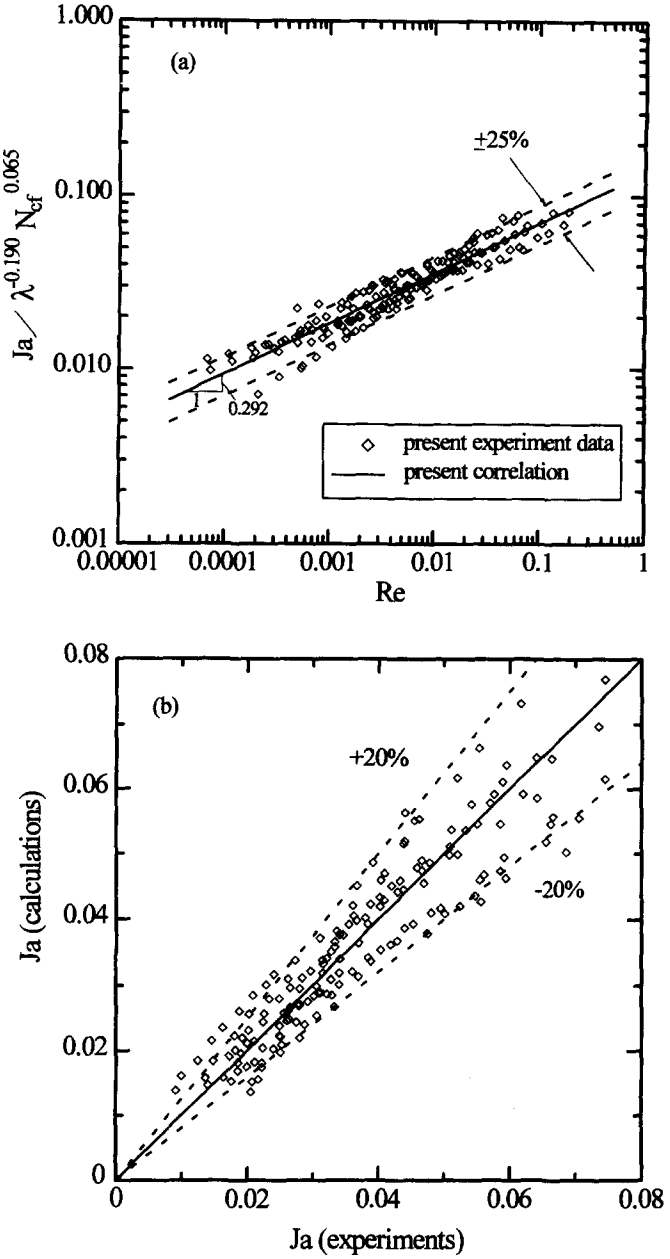

Fig. 9. The present correlation and its deviation with experimental data.

Following Rudemiller and Lindsay [16], a correlation for plasma and flame spraying surfaces of the present boiling data was developed. The major dimensionless groups according to [16] are the Reynolds number (Re), the Jakob number (Ja), the constant heat flux number (N_{cf}) and the geometric scale factor (λ). The correlation shown in Figure 9(a) has the following form of

$$Ja = 0.137[Re]^{0.292}[\lambda]^{-0.190}[N_{cf}]^{0.065}$$

$$6.909 \times 10^{-5} \leqslant Re \leqslant 1.899 \times 10^{-1}$$

$$6.667 \times 10^{-3} \leqslant \lambda \leqslant 1.667 \times 10^{-1}$$

$$7.773 \times 10^{-4} \leqslant N_{cf} \leqslant 4.787 \times 10^{-3} \qquad (2)$$

which is applicable to the plasma and flame spraying surfaces used in R-134a and R-407c. Figure 9(b) shows the performance plot for equation (2). The correlation predicts 95% of the data points within $\pm 20\%$. This correlation was derived by using standard procedures, and the dimensionless group Re ($= q\eta/h_{lv}\mu_l\varepsilon$) known as the Reynolds number represents a bubble agitation potential and Ja ($= C_{p_l}\Delta T/h_{lv}$)

will be familiar from other established boiling correlations. The third dimensionless group N_{cf} ($= \mu_l^2/\eta\rho_l\sigma$) stands for the ratio of the viscous force of the liquid-phase to the capillary force of the liquid phase. The last group is the geometric scale factor λ ($= \eta/\delta$) which describes the geometric configuration of the present porous matrix. Comparing the present correlation with Rohsenow's [17] for a smooth surface, one finds that the magnitude of the coefficient of the present correlation is 10–20 times larger than that of C_{sf} in Rohsenow's correlation and two additional terms (i.e. N_{cf} and λ) exist in the present correlation which are absent in Rohsenow's correlation; these are due to the present spraying coating porous matrix. The exponent of Re dependence is most likely to be for a similar reason; 1/3 for Rohsenow's correlation and 0.292 for the present case. However, due to the lack of adequate experimental data for pitted coating surfaces, the correlation for this type of surface seems unsuccessful and further study may be needed on this aspect.

CONCLUSIONS

Boiling in the presence of a metal porous medium from a horizontal surface for three different coating surfaces in two refrigerants (R-134a and R-407c) was extensively studied. The results lead to the following conclusions:

(1) Boiling heat transfer is enhanced by a thin layer of porous matrix coated on the heating surface, with an enhancement of up to 1.5 ~ 2.5 times. There seems to be an optimum surface roughness for heat transfer enhancement.

(2) In general, pitted coating surfaces (10c) give the best performance over a range of heat fluxes in R-134a. While the plasma spraying surface performs well (2p and 3p) in R-407c. The refrigerant properties seem to have a significant influence for these three different enhanced tubes.

(3) Boiling visualization provides a detailed understanding of phenomenological behavior by examining the bubble behavior of a typical enhanced surface (3p) compared to the corresponding smooth surface at the same heat flux level and in the same refrigerant.

(4) A correlation for plasma and flame spraying surfaces of the present boiling data with mean pore diameter and porosity of the substrate surface in terms of Reynolds number, Jakob number, constant heat flux number, and geometric scale factor was developed.

Acknowledgements—This work was supported by research grants (NSC 83-0413-E-110-002 and NSC 84-2212-E-110-018) from the National Science Council, Taiwan, Republic of China.

REFERENCES

1. Thome, J. R., *Enhanced Boiling Heat Transfer*. Hemisphere, New York, 1990, pp. 28–63.
2. Webb, R. L., *Principles of Enhanced Heat Transfer*. Wiley, New York, 1994, pp. 311–371.
3. O'Connor, J. P. and You, S. M., A painting technique to enhance pool boiling heat transfer in saturated FC-72. *ASME Journal of Heat Transfer*, 1995, **117**, 387–393.
4. You, S. M., Simon, T. W. and Bar-Cohen, A., A technique for enhancing boiling heat transfer with application to cooling of electronic equipment. *IEEE Transactions CHMT*, 1992, **15**, 823–831.
5. Hsieh, S. S. and Hsu, P. T., Nucleate boiling characteristics of R-114, distilled water (H_2O) and R-134a on plain and rib-roughened tube geometries. *International Journal of Heat & Mass Transfer*, 1994, **37**, 1424–1432.
6. Moffat, R. J., Describing the uncertainties in experimental results. *Experimental Thermal and Fluid Science*, 1988, **1**, 3–17.
7. Afgan, N. H., Jovic, L. A., Kovalev, S. A. and Lenykov, V. A., Boiling heat transfer from surfaces with porous layers. *International Journal of Heat & Mass Transfer*, 1985, **28**, 415–422.
8. Tehver, J., Sui, H. and Temkina, V., Heat transfer and hysteresis phenomena in boiling on porous plasma-sprayed surface. *Experimental Thermal and Fluid Science*, 1992, **5**, 714–727.
9. Bier, K., Engelhorn, H. R. and Gorenflo, D., Heat transfer with low-boiling halogene refrigerants, measurements taken with single tubes and transmission in tube nets. *Klima Kaelte Ing*, 1976, **11**, 399–406.
10. Stephan, K. and Abdelsalam, M., Heat-transfer correlations for natural convection boiling. *International Journal of Heat & Mass Transfer*, 1980, **23**, 73–87.
11. Cornwell, K. and Houston, S. D., Nucleate pool boiling on horizontal tubes: a convection-based correlation. *International Journal of Heat & Mass Transfer*, 1994, **37**, 303–309.
12. Malyshenko, S. P. and Styrikovich, M. A., Heat transfer at pool boiling on surfaces with porous coating. *Multiphase Flow and Heat Transfer, Second International Symposium*, Vol. 1, 1989, pp. 69–284.
13. Shi, M. H. and Liu, H. Y., The effects of thermal properties of the wall on nucleate pool boiling heat transfer. *Multiphase Flow and Heat Transfer, Second International Symposium*, Vol. 1, 1989, pp. 304–311.
14. Ko, S. Y., Liu, B. and Yao, Y. Q., Boiling hysteresis on porous metallic coatings. *Multiphase Flow and Heat Transfer, Second International Symposium*, Vol. 1, 1989, pp. 259–268.
15. Scurlock, R. G., Enhanced boiling heat transfer surfaces. *Cryogenics*, 1995, **35**, 233–237.
16. Rudemiller, G. R. and Lindsay, J. D., An investigation of boiling heat transfer in fibrous porous media. *Heat Transfer* 1990, *Proceedings of the Ninth International Heat Transfer Conference*, Vol. 5, 1990, pp. 159–164.
17. Rohsenow, W. M., A method of correlating heat transfer data for surface boiling of liquids. *Transactions of the ASME*, 1952, **74**, 969–876.